

# Geometric area measurements of circular apertures for radiometry at NIST

Joel Fowler and Maritoni Litorja

National Institute of Standards and Technology, Gaithersburg, MD 20899, USA

E-mail: litorja@nist.gov

Published 7 February 2003

Online at [stacks.iop.org/Met/40/S9](http://stacks.iop.org/Met/40/S9)

## Abstract

NIST has established a geometric aperture-area measurement facility for circular apertures. The instrument consists of an interferometrically controlled  $XY$  translation stage for high-accuracy positioning and a video microscope for detection of the edge of the aperture. Least-squares fitting of the edge points located along the aperture's inner circumference to the equation of a circle is used to determine the geometric area. In this paper we describe the measurement method, based on the work started and described by Fowler *et al* (1998 *Metrologia* **35** 497–500). Analysis and estimation of various contributions to the overall measurement uncertainty, including the effects of diffraction and partial coherence of light on the edge location, are also discussed.

## 1. Introduction

One of the limiting factors in the accuracy of many radiometric and photometric measurements is an accurate knowledge of the area of the aperture used to define the geometry. There are a variety of methods for dimensional metrology, mostly employing mechanical or electro-optical methods, or a combination of both, which can be used to accurately measure the area of an aperture. Currently, measurement methods use coordinate-measuring machines (CMMs) [1], laser techniques [2, 3], and relative flux transfer instruments [4] to measure radiometric apertures.

The system currently used at NIST is based on non-contact video-microscopy. Apertures made of a wide variety of materials can be measured. The instrument has been used to measure apertures with nominal diameters ranging from 1 mm to 50 mm, with both knife and flat edges. The general measurement procedure is to circumscribe the inner circumference using representative edge points. The  $x$ ,  $y$  coordinates of these edge points are used in a circle-fitting routine to determine the geometric area of the aperture. The circle-fitting model by Kasa, a variant of the least-squares fit method, is used here [5]. An ellipse-fitting model has also been used to assess the circularity of the aperture being examined [6].

## 2. System description

The system has been described previously [7]. It consists of a broadband light source illuminating the sample from

below through a Kohler illuminator, an air-bearing-supported, open-frame  $XY$  stage with a heterodyne laser interferometer feedback system for  $XY$ -axis positioning, a  $Z$ -axis translation stage carrying a microscope having objectives with a long working distance, a digital CCD camera and a control computer. Characterization of the whole system and all its components was performed before the measurement procedure; this included straightness of axis travel and squareness of the axes relative to each other [8]. Only microscope alignment is performed routinely.

## 3. Automated measurement procedure

The procedure is automated, requiring minimal involvement of an operator. The user needs to input the approximate radius of the aperture and the desired angular increments of the points to be determined. One measurement run with 72 sample points typically takes 40 min while 360 points take 80 min.

The sample aperture is placed on a custom-made mounting insert in the middle of the  $XY$  stage. The microscope, and hence the camera, views an edge segment by having the sample move in the  $x$  or  $y$  direction such that an edge point is at the centre of the camera's field of view. Distances travelled are measured by the displacement of the  $XY$  stage.

The procedure starts with the camera viewing any arbitrary section of the bright area (i.e. the internal portion) of the aperture. The stage then moves in the  $+x$  direction the equivalent of one field of view per move contiguously until a transition from light to dark (an edge) is within the field

of view. This is how the approximate location of the right edge (0°) is determined. The left, top and bottom edges of the circle are similarly located and approximate coordinates for the centre of the aperture calculated.

### 3.1. Edge point location

The grey levels of all pixels are read when searching for a transition. An edge point is then brought close to the centre of the field of view. The intensity, or grey levels, of the central array of pixels are scanned (a procedure called edge thresholding) horizontally if the edge point viewed is at or between 315° and 45° (right edge quadrant) and 135° to 225° (left edge quadrant), or vertically if it is between 45° and 135° (top edge quadrant) and 225° to 315° (bottom edge quadrant). Apportioning the edge points into these four quadrants allows thresholding for only the horizontal or vertical row of pixels. This is more convenient in writing the software and gave a level of uncertainty comparable to the more cumbersome method of sampling the pixels in the specific angular direction.

The pixels are labelled by integers, with the central pixel marked as the arbitrary reference point or origin. When an edge image is within the field of view, the *XY* stage is moved to bring the edge point to coincide with the central pixel. The number of pixels between the edge image's current pixel location and the centre is converted to actual *XY* stage travel using the pixel length and magnification. The pixel arrays are scanned again after the move to determine the new edge location. This process is repeated until the edge is at or close to the central pixel. The fine positioning is completed when the distance becomes less than 25 nm, the minimum incremental movement of the stage. A final edge thresholding is performed to determine the coordinates of the edge point (see figure 1).

Locating the exact position of the edge requires assignment of a particular level of light intensity to correspond to the edge. The average grey level counts of the dark area pixels are taken as the zero point and the average grey level counts in the bright area several micrometres away from the edge, hereafter referred to as *I*, is taken as unity. The light transition at the edge is not a step function, but rather has a finite width due to diffraction of light at the edge (see e.g. [9]). Theoretically, if the light in the image plane were totally incoherent the edge would be at the halfway point of the transition (0.5*I*), and if it were totally coherent it would be at the 0.25*I* point. The degree of spatial coherence in the image depends on the numerical apertures used in the imaging. In this set-up, the numerical apertures for both illumination and the objective are small, rendering the degree of partial coherence close to that of total coherence. Optical modelling software was employed to generate waveforms at an edge using optical constants for copper, a typical material for apertures. Various material edge thicknesses of less than a micrometre vertical wall were used in the calculations, assuming that the test aperture has a knife edge. For wavelengths from 400 nm to 700 nm, the calculated values ranged from 0.243*I* to 0.290*I*<sup>1</sup>. Assuming a rectangular distribution, which is reasonable given

<sup>1</sup> Optical waveforms at the edge are modelled using the *Metrologia* software, Spectel Research Corp., Mountain View, CA; the averaged intensity used for normalization is not the maximum intensity, since this value is not a reliable measure due to the overshoot and large pixel sizes; rather the asymptotic intensity level several micrometres away from the edge is used.

the profile of the filter used, the standard uncertainty in the assignment of the intensity at the edge is  $u = 0.014I$ . Figure 2 shows a simulated edge waveform and a sample edge waveform. Due to the chromaticity of the objective, there are out-of-focus contributions to the image that may account for the difference between the two curves. The effect on signal levels of scattering by rough features at the edge is not included in the modelling. The scattered light is assumed to be isotropic and contributing uniformly and is treated as background.

The coordinates of the edge point are determined more precisely by applying a subpixel length correction *C* to the stage position, as illustrated in figure 1. The location is determined by linearly interpolating between the values of pertinent vicinal pixels

$$X \text{ (or } Y) \text{ coordinate} = X \text{ (or } Y)_{\text{stage position}} \pm C. \quad (1)$$

The subpixel length correction *C* is determined as follows:

$$C = \frac{pL \cos(\sin)\beta}{M} \quad (2)$$

where *p* is the fraction of pixel the edge point is offset from the centroid of the central pixel and *L* is the pixel length in micrometres; cos (or sin) β, depending on whether thresholding is in the horizontal or vertical direction, accounts for the small angle between the *XY* axes of the stage and the *XY* axes of the camera and *M* is the magnification needed to translate analysed image distances to object distances.

The subpixel length correction is dependent upon the image being in focus. An unfocused, blurred image leads

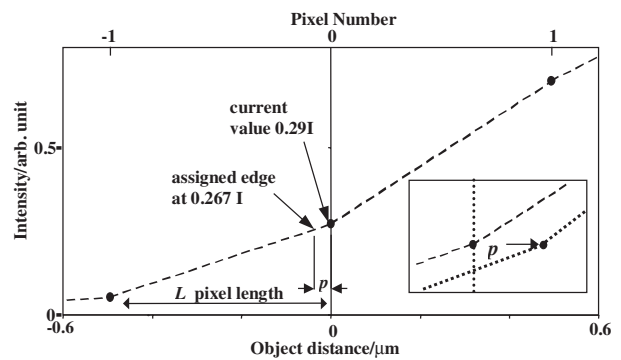


**Figure 1.** Illustration of the correction of subpixel length. After the final movement of the stage the edge might not be at the centre pixel. *p* is the fraction of pixel length, converted to object distance, that the assigned edge is offset from the centre.

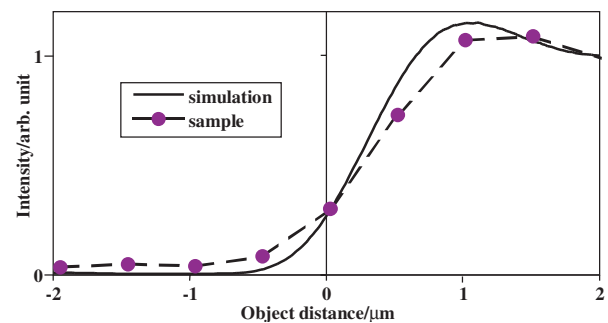


**Figure 2.** Simulated edge waveform versus sample edge waveform.

to an error in magnification and in the pixel location of the edge. In the measurements, an automated focusing routine is employed. Prior to the location of the edge points, an optimal focal plane for the sample under study is determined. The objective-to-sample distance at which the modulation transfer function (MTF) response of the optical system is at a maximum is the optimum focal location. This sharpness criterion was found to be robust, reproducible and unimodal [8]. An automated Fibonacci search algorithm is adopted to find the optimum objective-to-sample distance. Optimal focal locations are found at every 45° increment around the inner circumference of the aperture. This interval has been empirically found to be adequate in defining the optimal focal plane for the sample under examination. Optimum focal locations for those edge points to be measured in between the increments are found by linear interpolation.

#### 4. Uncertainty analysis

The uncertainty analysis used here conforms to the *Guidelines for Evaluating and Expressing the Uncertainty of NIST Measurement Results* [10]. The distance measured and obtained from the analytical fitting is the radius of a circle but the measurands in the experiment are the coordinates of each edge point. Thus, to determine the uncertainty in the radius, the uncertainties of the individual factors which determine the  $x$ ,  $y$  coordinates are estimated. According to (1) and (2), the coordinates of an edge point are as follows:

$$\begin{aligned} x(y)_{\text{coordinate}} &= f_{x(y)}(X(Y)_{\text{stage}}, p, L, \beta, M) \\ x(y)_{\text{coordinate}} &= X(Y)_{\text{stage}} \pm \frac{pL \cos(\sin)\beta}{M}. \end{aligned} \quad (3)$$

The uncertainty in determining the edge point coordinates depends upon five factors, the positional reading of the  $X$  (or  $Y$ )<sub>stage</sub>,  $p$ ,  $L$ ,  $\beta$  and  $M$ . Following the laws of propagation of errors, the standard uncertainty for the  $x$  coordinate in (3) is the sum of the squares of the uncertainties of each factor  $k$  weighted by its sensitivity coefficient. A similar equation is generated for the  $y$  coordinate

$$u_{(x)}^2 = \sum_{i=1}^5 \left[ \frac{\partial f}{\partial k} \right]^2 u^2(k). \quad (4)$$

A list of the various sources of uncertainty, their type and contributions to the total uncertainty is presented in table 1. The first three columns present estimated values for a small and large aperture while the last two columns present results from 10 ( $n = 10$ ) repeat 360-point measurements of a copper knife-edged aperture sampled at 1° intervals. The sample was not moved between measurements so that approximately the same edge points were sampled in each run.

The random type A uncertainty on a single  $x$  or  $y$  coordinate measurement is approximately 50 nm. This is due to random uncertainty in stage position and a small contribution from random fluctuations in the source and detector. This contribution decreases with the number of sample points. In the sample measurements, the standard deviation of the mean radius was found to be less than 20 nm; this is due to random uncertainty of the stage and the imaging system, but can also include uncertainty of aperture form (i.e. imperfections).

The systematic uncertainty in the readings of the stage position is estimated to be  $2.6 \times 10^{-6}$  mm mm<sup>-1</sup> of axis travel. This estimate is based on the type of stage and interferometer system used and assuming a rectangular distribution with  $10^{-5}$ – $10^{-6}$  as the interval limits. This uncertainty scales with the longest distance travelled by the stage, which for these measurements is the diameter of the aperture.

The sources of the systematic uncertainty in the imaging system are listed in table 1 with their nominal contributions to the estimated uncertainties. The uncertainty in  $p$  is the root sum of squares of various factors that affect the detection of the edge by the imaging system: the edge assignment using intensity, which is referred to as the coherence factor, the uncertainty in focus and uncertainty due to off-axis thresholding, since we are thresholding only the horizontal or vertical pixel arrays.

The combined uncertainty for the  $x$  coordinate, shown in (5), is the root sum of squares of the random ( $u_i$ ) and systematic ( $u_j$ ) uncertainties of the stage and imaging system. A similar equation is generated for the  $y$  coordinate:

$$u_{c(x)} = [u_{i(x)\text{stage}}^2 + u_{i(x)\text{image}}^2 + u_{j(x)\text{stage}}^2 + u_{j(x)\text{image}}^2]^{1/2}. \quad (5)$$

The estimated combined uncertainty due to instrumental uncertainties is shown in (6). There is a factor of 2 since two edge points are needed to determine a radius. In these

**Table 1.** List of the sources of uncertainty in the determination of each edge point, their type and estimated contributions to the total relative uncertainty in area for  $R = 0.5$  mm and 25 mm; measurement results for an aperture with  $R = 2.6$  mm.

Source of uncertainty and type	Estimate value/ nm	$R = 0.5$ mm $u(A)/A$	$R = 25$ mm $u(A)/A$	Value/ nm	$R = 2.628\ 257$ $u(A)/A$
Stage, random (A)	50	$2.0 \times 10^{-4}$	$4.0 \times 10^{-6}$	13	$9.9 \times 10^{-6}$
Stage, systematic (B)	$2.6 \times 2R$	$1.0 \times 10^{-5}$	$1.0 \times 10^{-5}$	13.7	$1.0 \times 10^{-5}$
Image, random (A)	2	$8.0 \times 10^{-6}$	$1.6 \times 10^{-7}$		
Image, systematic (B)	4			4	$3.0 \times 10^{-6}$
$p$ pixel fraction					
focus		$2.4 \times 10^{-7}$	$4.8 \times 10^{-9}$		
coherence factor		$1.3 \times 10^{-5}$	$2.7 \times 10^{-7}$		
off-axis threshold		$2.3 \times 10^{-6}$	$4.7 \times 10^{-8}$		
$L$ , pixel length		$3.8 \times 10^{-9}$	$7.6 \times 10^{-11}$		
$\beta$ , stage/CCD angle		$8.9 \times 10^{-15}$	$1.8 \times 10^{-16}$		
$M$ , magnification		$4.5 \times 10^{-8}$	$9.0 \times 10^{-10}$		
Thermal change (B)	$8 \times R$	$1.7 \times 10^{-5}$	$1.7 \times 10^{-5}$	3	$6.6 \times 10^{-6}$
Artefact geometry (B)	$0.08^\circ$	$2.0 \times 10^{-6}$	$2.0 \times 10^{-6}$	$0.06^\circ$	$1.1 \times 10^{-6}$
Total $u(A)/A$ ( $k = 1$ )		$4.0 \times 10^{-4}$	$2.7 \times 10^{-5}$		$2.5 \times 10^{-5}$

calculations, all values for instrumental uncertainties are nominally the same for both  $x$  and  $y$

$$u_{c(xy)} = [2u_{c(x)}^2 + 2u_{c(y)}^2]^{1/2}. \quad (6)$$

All dimensions reported are the dimensions of the sample at 20 °C and a correction is made according to (7), where  $t$  is the average temperature during the measurement and  $\alpha$  is the coefficient of thermal expansion. An environmental monitor situated close to the sample stage measures the temperature before and after each measurement run. The initial and final temperatures have been observed to vary by 0.5 °C at most, but more typically by 0 to 0.2 °C. The uncertainty in dimensions  $u_{j(t)}$  due to the uncertainty in the temperature is shown in (8). An estimate of the uncertainty of  $\alpha$  cannot be provided at present, and in the uncertainty calculations only the first term is used. Measurements taken with the sample temperature close to 20 °C will minimize the second uncertainty term in (8)

$$\Delta R = (20\text{ °C} - t)\alpha R \quad (7)$$

$$u_{j(t)} = [(\alpha R u_t)^2 + (R(20 - t)u_\alpha)^2]^{1/2}. \quad (8)$$

The sample is mounted on custom-made inserts such that the aperture is coplanar with the measurement axes. There is uncertainty in the flatness of the insert that could lead to an angular variation or tilt of the aperture plane with respect to the  $XY$  stage. An estimated angle of 0.08° is used in the estimations based on the uncertainty in the tool machining equipment used to manufacture the inserts. At present, the maximum difference in the optimum focal locations is used as a tool in determining whether a sample is mounted as flatly as possible.

The estimated total uncertainty in the measured radius (9) is the sum of the squares of the random uncertainty in the  $x$  and  $y$  axes of the stage position ( $u_{i(xy)\text{stage}}$ ) and imaging ( $u_{i(xy)\text{image}}$ ) and systematic uncertainties  $u_{j(xy)\text{stage}}$  for the stage and  $u_{j(xy)\text{image}}$  for the imaging, thermal variation  $u_{j(t)}$

and artefact geometry  $u_{j(g)}$  terms:

$$u(R) = [4u_{i(xy)\text{stage}}^2 + 4u_{i(xy)\text{image}}^2 + 4u_{j(xy)\text{stage}}^2 + 4u_{j(xy)\text{image}}^2 + u_{j(t)}^2 + u_{j(g)}^2]^{1/2} \quad (9)$$

$$u(A) = 2\pi R u(R). \quad (10)$$

For an aperture with radius  $R = 0.5$  mm,  $u(R)$  is estimated to be 100 nm, and for one with  $R = 25$  mm,  $u(R)$  is estimated to be 348 nm. The relative uncertainties in area are  $4.0 \times 10^{-4}$  and  $2.8 \times 10^{-5}$  ( $k = 1$ ), respectively. In summing the relative uncertainty in area for the test sample in the last column of table 1, the random uncertainty obtained from the measurements is uncertainty in the radius, not of edge points as in (9), so that the multiplication factor of 4 is not necessary.

### Acknowledgments

The authors wish to acknowledge the work done by R Durvasula in the development of the measurement data acquisition and control software and to B C Johnson and G Fraser for their technical comments.

### References

- [1] Martin J, Fox N, Harrison N, Shipp B and Anklin M 1998 *Metrologia* **35** 461–5
- [2] Fischer J and Stock M 1992 *Meas. Sci. Technol.* **3** 693–8
- [3] Lassila A, Tovanen P and Ikonen E 1997 *Meas. Sci. Technol.* **8** 973–7
- [4] Fowler J and Deszi G 1995 *J. Res. NIST* **100** 277–83
- [5] Kasa I 1976 *IEEE Trans. Instrum. Meas.* **25** 8–14
- [6] Albano A 1974 *Comput. Graphics Image Process.* **3** 23–33
- [7] Fowler J B, Durvasula R S and Parr A C 1988 *Metrologia* **35** 497–500
- [8] Durvasula R 1999 *PhD Thesis* Tufts University
- [9] Born M and Wolf E 1999 *Principles of Optics* 7th edn (Cambridge: Cambridge University Press) p 972
- [10] Taylor B N and Kuyatt C E 1994 *NIST Technical Note* **1297** 20